

# Validation of a finite element model for axle box acceleration at squats in the high frequency range



Maria Molodova, Zili Li\*, Alfredo Núñez, Rolf Dollevoet

Section of Railway Engineering, Faculty of Civil Engineering and Geosciences, Delft University of Technology, Stevinweg 1, 2628 CN Delft, The Netherlands

## ARTICLE INFO

### Article history:

Received 24 July 2013  
Accepted 12 May 2014

### Keywords:

Axle box acceleration  
Squats  
Finite element method  
Dynamic simulations  
Railway track inspection

## ABSTRACT

Squats are associated with high frequency vibrations of the wheel–rail system and can be registered using axle box acceleration (ABA) measurements. In this paper a three-dimensional finite-element (FE) model is proposed to capture the dynamic features of the ABA related to squats in the high frequency range. The FE model is validated relying on a set of real-life ABA measurements at two characteristic rail surface defects (light and severe squats), located in a section of the railway network in Assen. The Netherlands. The FE model managed to properly capture the dynamic features in the range of frequencies up to 2000 Hz.

© 2014 Elsevier Ltd. All rights reserved.

## 1. Introduction

Squats are rolling contact fatigue defects in rails, generally considered as surface-initiated short track defects [1,2,3]. One of the characteristics of mature squats is localized depression of the contact surface of the rail head that can have a shape of two lungs (Fig. 1b and c). Other of their characteristics are the widening of the running band and corrugation-like wave pattern following the squat, as a result of plastic deformation or wear caused by the impact of the dynamic wheel–rail interaction. As a way to systematize the visual inspections of squats, in Smulders [3] it is proposed to subdivide squats into three classes: class A for light squats, class B for moderate squats, and class C for severe type of squats. In Fig. 1, some reference photographs used to identify the three classes of squats are shown.

Squats may initiate at a small indentation [3,4,5]. Squats are also associated with corrugation and welds [5]. A detailed analysis of the process of development of a typical squat starting from an indentation was presented in [6] and validated by field measurements in [1]. Cracks of V, U, Y or circular shape usually form at mature squats [1,2,6], propagate inside the rail head at a shallow angle to the surface, and grow till about 3–6 mm deep in the sub-surface, before they branch downward transversely [7]. It is believed that the dynamic force at a local geometrical irregularity on the rail surface (for example, at an indentation) is the cause of the initiation and development of the cracks [1,5,6]. Since the

indentations usually do not have cracks at the beginning, the light squats may also have no cracks. Fig. 1a shows a pre-crack state of a light squat.

Currently the detection of squats still relies heavily on human inspection. In The Netherlands, these inspections are undertaken twice-yearly by maintenance contractors, and aim to determine the precise location and severity of the squats. The main problems of human inspection for the detection of squats are not just that it is very labour intensive and expensive, but also that in most of the cases it is just not feasible by manually inspections to detect early anomalies. Nowadays, the treatments to solve these defects are very often at a severe stage of degradation, leading sometimes to the rail replacement because the cracks may grow in the subsurface and cause rail break. For that reason, it is very important to detect the early stage squats when the resulting degradation is still light because they can be well controlled and treated by for example grinding away a thin layer from the rail surface. Therefore, methods for early detection of squats are relevant not only for a cost effective maintenance policy, but also because the prevention of disruptions and derailment is of paramount importance for railway infrastructure managers in order to guarantee a safe and robust performance of the railway network.

There are different types of sensors to perform a track inspection for squats detection, each with its own advantages and disadvantages. For example, recently, Peng and Jones [8] proposed the use of an infrared camera for detecting squats in track using measurement of the thermal wave variation in phase or amplitude. To evaluate the method, they proposed the use of a 3D finite element modelling to simulate the lock-in thermography

\* Corresponding author. Tel.: +31 152782325; fax: +31 152783443.  
E-mail address: [z.li@tudelft.nl](mailto:z.li@tudelft.nl) (Z. Li).

process. In the current paper, the focus is on the use of axle box acceleration (ABA) measurements, which can indicate not only short track defects like squats, but also corrugation, welds and insulated joints with poor quality, among other rail health conditions.

Regarding the use of ABA, Bocciolone et al. [9], Massel [10] and Caprioli et al. [11] discussed a track diagnostic tool using ABA measurements for detection of short pitch corrugation. Remennikov and Kaewunruea [12] discussed the application of ABA for the detection of vertical impact force at corrugation, and relation between ABA and wheel flats. However, corrugation and a wheel flat are much easier to detect than a squat, because the first one is distributed over a long length of rail, and the second one cause periodic responses in ABA signals, while a squat often appears as an isolated rail defect. In Molodova et al. [13] and Li et al. [14] it was shown that ABA measurements can be applied for the detection of isolated short wave rail surface defects. The effectiveness to detect squats by using the magnitude of the ABA measurement as identification feature was assessed in terms of hit rate, which is the ratio of detected irregularities over the total number of irregularities. The hit rate of detection of severe squats by high values of magnitude in the ABA measurement was 100%, while the hit rates of moderate and light squats were 60% and 57% respectively, which is yet too low for a trustable preventive method to be integrated into a real-life decision support system. As the temporal analysis of the measurements was not sufficient, in this paper the high frequency content of ABA measurements at squats is investigated. Since it is difficult to acquire from real-life tests all the necessary data under well-defined conditions for feature extraction, the purpose of the current paper is to propose the use of a dynamic model, which is capable to reproduce the temporal and frequency characteristics of axle box acceleration (ABA) measurements at squats.

In the literature different approaches have been used to model the train-track interactions [15,16,17,18,19,20]. In this paper the use of a three-dimensional finite element (FE) model is proposed for numerical reproduction of axle box acceleration (ABA) at squats capable to properly simulate the real-life temporal and frequency characteristics. The detailed modelling of the wheel–rail contact guarantees that the high-frequency contact interaction at a geometrical irregularity, representing a squat, is accurately considered. In [6] it was found that the wavelengths of the contact force at squats are mainly between 20 mm and 40 mm, which correspond to 1000–2000 Hz for a rolling speed of 40 m/s, the typical speed of Dutch passenger trains. Since ABA is a measure of vibration of the coupled vehicle-track system, it is expected that the same frequencies can be observed in ABA signals of squats. Then, by comparing the respective frequency characteristics in the normal state with the ones with squats, the location and the severity of the squats can be assessed. In Molodova et al. [13], the ABA responses at squats were simulated with the FE model and validated by the measurements only in the frequency range up to 1 kHz, because the available ABA measurements were filtered with low-pass filter with cut-off frequency of 1 kHz. In this paper all the proper cautions were taken to ensure that high frequency ABA responses were measured and the validation of the FE model is

focused on the frequency range up to 2 kHz. This feature makes the proposed model a flexible tool to study relationships between ABA and squats, and the influence of other track parameters. Then, the design of robust monitoring system and early squats detection methods can be addressed relying on this FE model, and further developments can be implemented and validated by track inspection.

## 2. Finite element (FE) model

A scheme of the developed FE model for simulations of dynamic interaction at squats is shown in Fig. 2. To simplify it and reduce the calculation time, the model included only a half of the wheelset with sprung masses of the car body and the bogie, and a half of the track, taking advantages of the system of straight track and the shortwave characteristics of the high frequency vibration. The half wheelset, the rail and sleepers were modelled with three-dimensional brick solid elements, representing their real geometry and material properties. The wheel flange was ignored, as the contact is between the wheel tread and the rail crown. The primary suspension, rail pads and ballast were modelled as springs and dampers. The length of the model is 10 m. The rail profile was 54E1 with 1:40 inclination. The wheel was considered with nominal wheel radius of 0.46 m and wheel thread concavity of 1:40. Since squats usually occur on the rail top, some irrelevant details of the wheel geometry were ignored, such as the wheel flange. The parameters of the model listed in Table 1 are the nominal parameters of the Dutch railway track. Note that the value of  $K_2$  corresponds to a very stiff pad. This stiffness value is in agreement with measurements and studies performed in Dutch railway tracks, as can be seen in [21,22]. In this model the effects of sub ballast and foundation layers are not considered, as their influences are not in the range of interested frequencies for detection of squats [23], which is higher than 200 Hz. The material model for the wheel and rail was linear elastic with Young's modulus 210 GPa and Poisson's ratio 0.3, while for the surface layer of the rail, to take into account of the plastic deformation at squats, the material was bi-linear elastic–plastic with yield stress 0.8 GPa including material hardening and tangent modulus 21 GPa. Rayleigh stiffness-proportional damping coefficient of 0.1 was used for materials of wheel, rail and sleepers.

A squat was modelled as a vertical deviation of the rail surface. The model of the squat was applied to the nominal rail surface by vertically shifting the surface nodes of the rail. The deepest point of the squat was located at a distance  $L$  relative to the sleeper, given by the position of the simulated squat in the track (see Fig. 2a). For the 3D solid elements modelling, the wheel and rail were densely meshed at the contact surfaces (Fig. 2b). The detailed modelling of the vehicle-track system around the contact will guarantee that the rolling contact between the wheel and rail as continua are accurately treated, and to be able to capture the related interaction between the wheel and the track as structure. The smallest element size on the wheel and rail contact surfaces was about 1.3 mm. The mesh of the rail in the longitudinal direction was fine

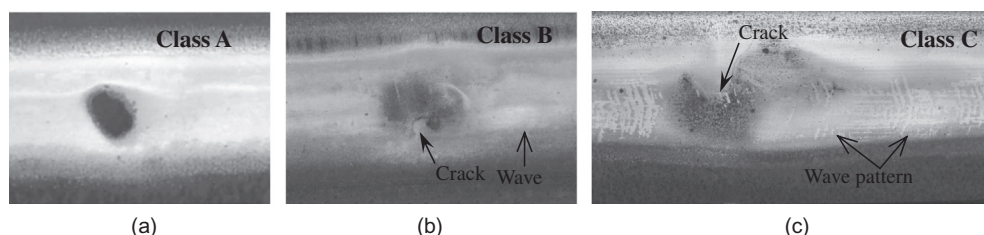
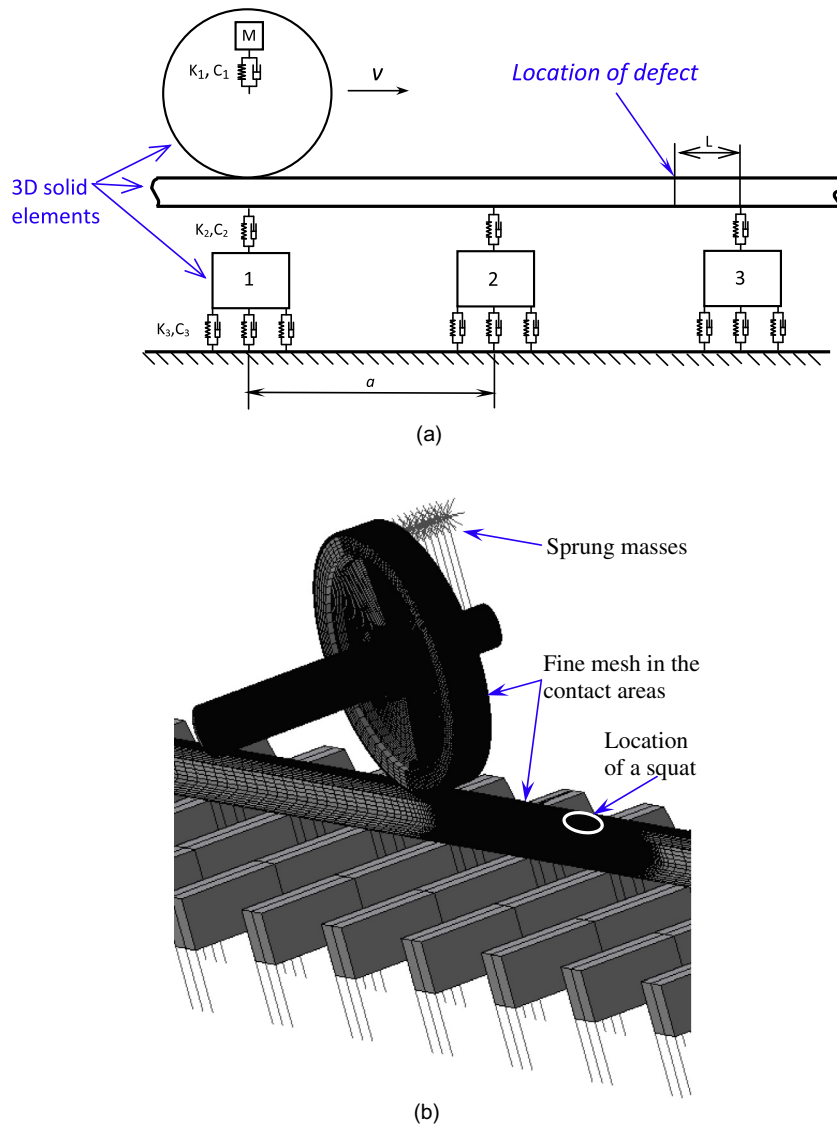


Fig. 1. Classes of squats (a) class A or light squat, (b) class B or moderate squat, (c) class C or severe squat.



**Fig. 2.** The FE model. (a) The scheme of the model. The parameters  $K_i$ ,  $C_i$  and  $M$  are listed in Table 1;  $v$  is the speed of the wheel. The location of a rail surface defect is shown with an arrow. (b) The FE model visualized in 3D.

**Table 1**  
Parameters of the model.

Component	Parameter	Symbol	Value
<i>Track parameters</i>			
Rail pad	Stiffness	$K_2$	1300 MN/m
	Damping	$C_2$	45 KNs/m
Sleeper	Mass		244 kg
	Sleeper distance		0.6 m
Ballast	Stiffness	$K_3$	45 MN/m
	Damping	$C_3$	32 KNs/m
<i>Vehicle parameters</i>			
Sprung mass	Mass	$M$	8000 kg
First suspension	Stiffness	$K_1$	1.15 MN/m
	Damping	$C_1$	2500 Ns/m
<i>Wheel and rail</i>			
Material	Young's modulus		210 GPa
	Poisson's ratio		0.3
	Mass density		7800 kg/m <sup>3</sup>
	Yield stress		0.8 GPa
	Tangent modulus		21 GPa

(1.3 mm) around the starting position of the wheel and around the defect. Between the starting point and the defect the largest longitudinal element size was 5 mm, with intermediate transitional element sizes between the smallest and the largest sizes. The part of the rail which is considerably far away from the defect was meshed with an element size of up to 7.5 cm. When those elements were reduced from 7.5 cm to 3.75 cm, only very small effects on the magnitude and the wavelength of ABA at squats were observed. The number of elements in the model is 344,816 and the number of nodes is 395,525.

The dynamic response of the model is obtained with a combination of an implicit integration part for calculation of the static equilibrium of the wheel–track system, and an explicit integration part for dynamic simulations of the wheel rolling over the rail. The first step of the solution procedure is the static analysis. An implicit integration method was used to close the gap between wheel and rail, to find their equilibrium position and calculate the initial deformation of the wheel–track system. The second step is the dynamic analysis, when the wheel ran over the rail towards the

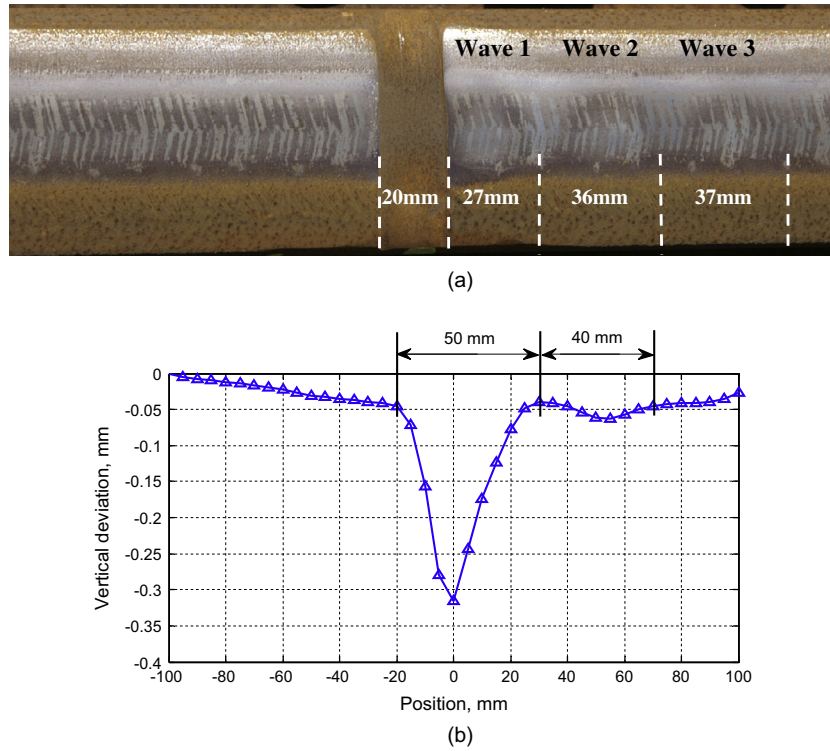


Fig. 3. Light defect under controlled contact conditions. (a) Photo of the defect. (b) The vertical–longitudinal profiles of the artificial defect.

squat. The displacements obtained from the implicit analysis define the initial state of the explicit analysis when stress initialization is performed. An initial speed of 30 m/s (the same speed as the measurement train) was applied to the wheel and the lumped mass that represents the mass of the bogie and the car body, which are above the primary suspension. To define the rolling speed of the wheel, an angular velocity of 65.2 rad/s was considered. To control the creepage, a torque of 12,450.49 Nm about the rolling axis was applied to the wheel. The first part of the dynamic analysis, with a distance of 1 m travelled by the wheel before reaching the defect (relaxation distance), was used to damp out the initial vibration excited by imperfect static equilibrium obtained by the static analysis. This dynamic relaxation is necessary because of the high contact stiffness of the wheel–rail contact; small error in the calculated displacement will cause large imbalanced stress, causing initial vibration. The central difference integration scheme was used for explicit integration. The time step

of 0.02295 ms was determined by the Courant criterion [24]. The contact between wheel and rail was modelled using surface-to-surface algorithm [25]. The penalty method was used for solution of the contact problem. The Coulomb friction law was employed with a friction coefficient of 0.3.

In the next sections, to validate the proposed model two defects were simulated. The first one is a rail head cut in the transverse direction. This artificial defect with a uniform lateral geometry and the length of a typical light squat was produced in the in-service track to simulate ABA under controlled contact conditions. The second simulated defect is a severe squat with more complicated contact conditions. The analysis includes the comparison of the simulated ABA with the ABA measurements in both the temporal and the frequency domains, with a focus on high frequency responses. For both, Sections 3 and 4, the parameters of the explicit integration and contact algorithms are the same as described before.

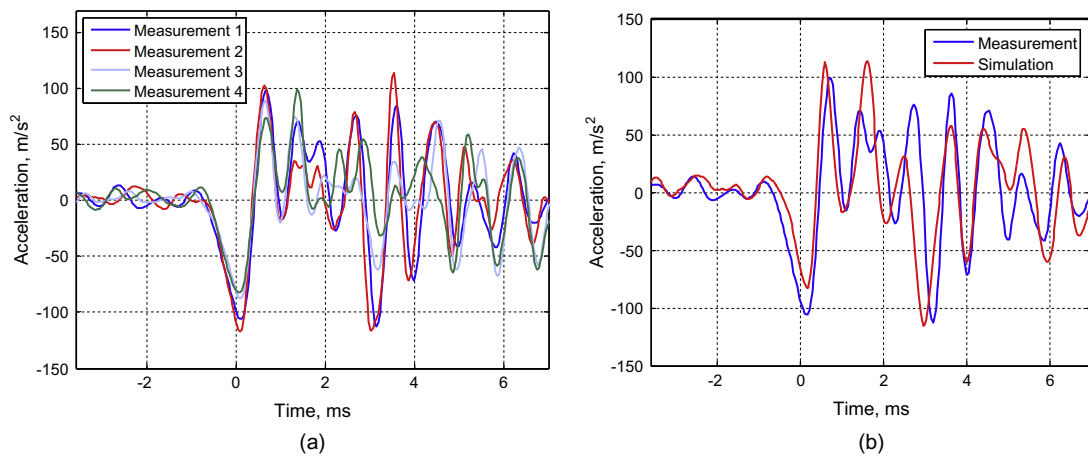


Fig. 4. Calculated and measured ABA. (a) Measured ABA. (b) Calculated and measured ABA.

### 3. A light defect under controlled contact conditions

#### 3.1. Geometry of the defect

In [13] it was shown that the wheel–rail interaction at a rail defect is influenced by the lateral geometry of the defect. For a number of ABA measurements the measuring wheel may run across the defect at different positions of it because of the lateral displacement of the wheelset relative to the rail due to, e.g. hunting. This factor becomes even more influential when the size of the defect is smaller than the width of the rolling band, because in such a case not every wheel passage will run over it.

To ensure that the contact conditions are the same in each run of the measuring train, an artificial defect, which was uniform in the lateral direction in terms of width and depth, was made on the rail in Assen, The Netherlands. The length of the artificial defect was 20 mm, which is typical of light squats. The purpose of the simulations of this section is to validate the ABA calculated with the FE model, provided that the lateral geometry of the defect does not influence the calculated and measured results.

Fig. 3a shows a photo of the artificial defect, taken three months after it was made. The traffic direction was from left to right. It can be clearly seen that the wave pattern caused by the fluctuation of the contact force has already appeared to the right side of the defect. It has the wavelength of 20–40 cm, which is typical of squats. This range for the length of the wave pattern has been extensively verified through numerical work and later verified with field observations in [1]. On the right side of the artificial defect the widening of running band is seen, which is also typical of the corrugation-like pattern following squats. Therefore, this defect is similar to squats in terms of dynamic interaction.

The vertical–longitudinal profile of the rail around the artificial defect was measured with the RAILPROF device. RAILPROF measures rail profiles within 1 m on the centre line of the rail. Fig. 3b shows the rail vertical–longitudinal profile measured at the artificial defect. The size of the artificial defect is about 50 mm. This equals approximately to the length of the cut together with the first wave in Fig. 3a. The next wave in Fig. 3b is about 40 mm which corresponds to the second wave on the rail surface in Fig. 3a. The discrepancies between the wavelengths of Fig. 3a and b can be owing to two factors. The first is that the wave pattern has somehow a different vertical–longitudinal profile when it is measured at different lateral position of the rail. The second factor is that the longitudinal resolution of the profile measurements was only 5 mm.

#### 3.2. Validation of ABA magnitude at the light defect

The ABA signals were measured with accelerometers mounted on the four axle boxes of a bogie of the train. The sampling frequency of ABA measurements was 25 kHz. In the post-processing, the ABA measurements were low-pass filtered with the cut-off frequency of 2 kHz, since it was observed from the ABA measurements that this frequency range is related to squats. The ABA measurements were repeated several times on the same track (see Fig. 4a). The dispersion of the ABA measurements in the magnitudes of the first peak caused by the rail defect was about 28%. The dispersion is probably caused by hunting oscillations. The wavelength of the first two peaks in ABA signals agreed well in all the measurements. Since the wavelength is related to the major frequencies components of ABA, and it does not deviate much in the measurements, the frequency content of ABA could be the better characteristic for detections of squats, rather than the ABA magnitude. Repeated measurements were important due to the following reasons. First of all, to examine the repeatability of the

ABA measurements at the short track irregularities because they should have similar response for every measurement within one day. The second reason to repeat the measurements is to increase the probability to detect light squats. The wheel–rail interaction at a squat is influenced by the lateral geometry of the squat. However, during the several measurement runs a wheel might have travelled along different trajectory on the rail because of the hunting oscillation. ABA measurements at the investigated artificial defect were obtained about one month before the profile of Fig. 3b was measured. The speed of the measuring train varied between 27 and 30 m/s at different runs at that location. Since the rolling speed was not exactly the same, that can cause the difference in the wavelengths of the signals. To eliminate such differences, the measured signals were compared in time domain.

Fig. 4a shows four ABA measurements at the artificial defect, made on the same day. These measurements coincide very well by magnitude in the first peak and wavelength, except for the second peak after the excitation around 1.4–2 ms, the fourth peak around 3.5 ms and the sixth around 5 ms. Since the measurements are very well repeated, only one measurement (Measurement 1) will be considered for comparison with calculated results.

A comparison between measurement 1 and the calculated ABA by simulation is shown in Fig. 4b. The maximum measured ABA is  $100 \text{ m/s}^2$ . The maximum calculated ABA is  $115 \text{ m/s}^2$ . Hence, the maximum calculated ABA is coherent with the measurement. The calculated and the measurement are generally similar in wavelength, while there are some differences in magnitude. The difference in magnitudes may have been influenced by the geometry of the defect, or by some random factors of the wheel–track system. Note that there was also some difference in the measured ABA at these points (see Fig. 4a). It is noticed that the difference at the second peak and the sixth peaks are related to vibration components of shorter wavelength. It is also noticed that these shorter wavelength components appear in measurement 2 at both the second and the sixth waves, while they are observed only in the second wave in measurement 1 and in the fifth wave in the simulation.

The ABA response to the defects is a combination of forced and free vibrations of the system. The cut in the rail of 20 mm long (Fig. 3a) produced the forced vibration part of ABA. The length of the next wave on the rail surface is 27 mm. This wave was produced partly by forced and partly by free vibrations of the system. The wavelength of the following wave pattern is 36–37 mm, which were formed by free vibrations.

The average wavelength of the calculated ABA after the impact is, however, only about 29 mm (Fig. 4b). This is because the speed of the measuring train and simulations was about 30 m/s, which is lower than the speed of the normal traffic, 40 m/s, which is responsible for the formation of the wave pattern on the rail surface. When the corresponding frequencies are looked at, they are 1034 Hz for 29 mm at 30 m/s and 1081 Hz for 37 mm at 40 m/s. The difference between these two frequencies is less than 5%.

#### 3.3. Methods for the frequency analysis

There are different techniques available for the investigation of frequency characteristics of a signal. One to investigate local frequency characteristics is the Short-Time Fourier Transform (STFT), which is a good method for the analysis of ABA measurements at squats. In this technique the observed function is multiplied by a moving window function, and then Fourier Transform (FT) is calculated. Since multiplication by a relatively short window gives an indication of the frequency content of the signal in the neighbourhood of the analysis point and effectively suppresses the signal outside this area, the STFT represents a local spectrum of the signal

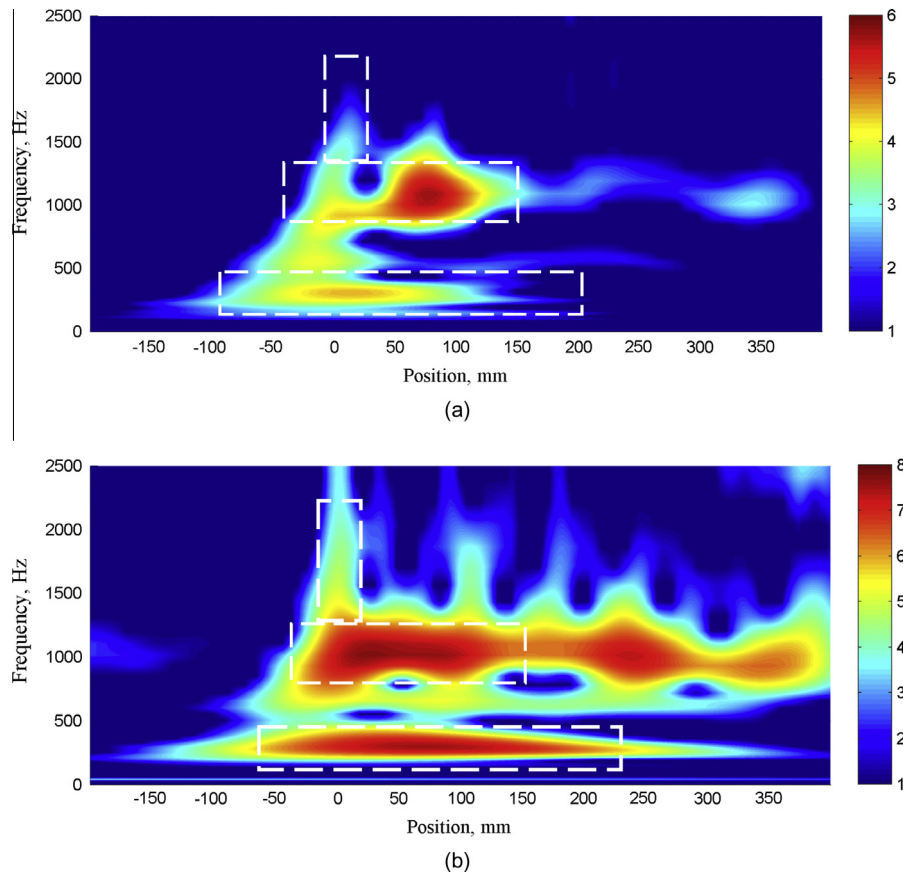


Fig. 5. Wavelet power spectrum of measured (a) and calculated (b) ABA.

around the analysis time [26]. However, this method has a drawback. The time–frequency representation by this method depends on the window size. When the window is narrow it can provide a good time resolution with poor frequency resolution; while when the window is wide it can provide good frequency resolution and poor time resolution.

Another technique, the wavelet analysis, has the advantage that the time–frequency representation is not dependent on the window size. Continuous wavelet transform (CWT) is a time–frequency analysis tool, where the observed function is multiplied by a group of shifted and scaled wavelet functions. CWT can be defined as follows [27]:

$$W_x(s, \tau) = \frac{1}{\sqrt{s}} \int_{-\infty}^{\infty} x(t) \psi^* \left( \frac{t - \tau}{s} \right) dt, \quad (1)$$

where  $x(t)$  is the analysed signal,  $\psi(t)$  is a locally defined function called mother wavelet (the Morlet function is used), the term  $\frac{1}{\sqrt{s}} \psi \left( \frac{t - \tau}{s} \right)$  is a family of wavelets deduced from the mother wavelet by different translations  $\tau$  and scaling  $s$ , \* indicates a complex conjugate,  $s > 0$  is the wavelet scale,  $\tau$  is the translation, and  $W_x(s, \tau)$  represents the wavelet coefficients for the signal.

The main advantage of CWT compared to STFT is a very good level of time and frequency resolution. Therefore, wavelet analysis is appropriate for investigation of non-stationary phenomena with local changes in the frequency components, such as structural damage detection and crack identifications [28,29,30,31]. The power spectrum of a wavelet transform is defined as the sum of the square of wavelet coefficients. The plot of wavelet power spectrum (WPS) is called a scalogram. A vertical slice of a wavelet plot is a measure of the local spectrum.

### 3.4. Validation of frequency characteristics of ABA at the light defect

Considering the forced vibrations caused by the defect with the length of 20 mm, frequencies up to 1500 Hz are expected in ABA signals with the measuring and simulation speed of 30 m/s. For the normal traffic speed (about 40 m/s) the frequency at the impact should be up to 2000 Hz (and even higher for smaller defects).

The major features in the wavelet power spectrum of the measured and the calculated ABA are in agreement, as can be seen in the Fig. 5. The red colour around zero position represents high energy of the signal caused by an impact at the defect. At the moment of the impact (around zero position) frequencies up to 1700 Hz can be observed in the measured signal and up to 2500 Hz in the calculated one. The high frequency response of very short duration corresponds to the forced vibration of the system. It is assumed that the strong responses of the longer duration around frequencies of 300 Hz and 1000 Hz, indicated with the horizontal rectangular boxes, correspond to free vibrations of the system. The nature of these vibrations will be further investigated in future work.

Power spectral density (PSD) describes the distribution of the power of a signal along the frequencies. PSD of the measured and calculated signals are shown in Fig. 6. Power density of the simulated ABA is higher than the measured ones in the two most important peaks. The first major frequency is at about 300 Hz and it is similar to the one found in both the measurements and the simulation. The second major frequency at about 1000 Hz is somehow higher than those of the measurements. This difference can be caused by local deviation of the track parameters from the nominal ones which were used in simulations. The other two frequencies at about 500 and 700 Hz do not appear in each measurement, while

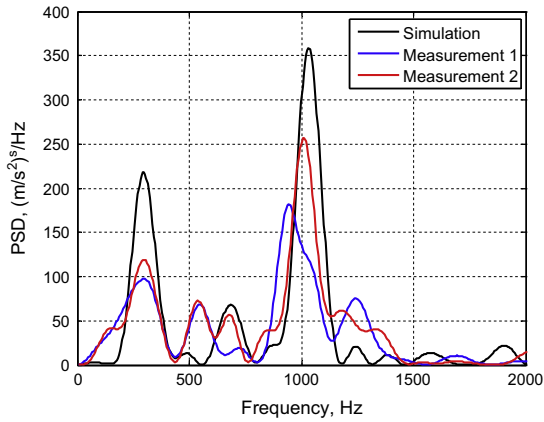


Fig. 6. PSD of measured and calculated ABA.

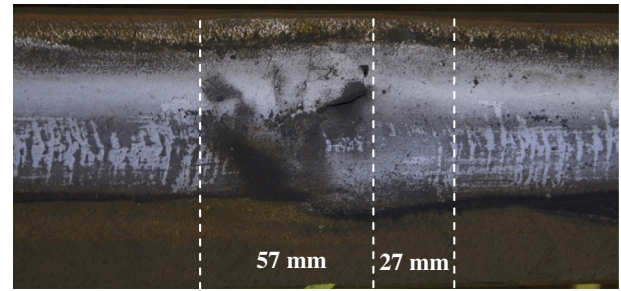
one of them was reproduced in the simulation; this indicates the randomness aspect of the measurement, and the difficulty for simulation to match all the details of measurements. There are also a number of peaks in the PSD between 1200 and 2000 Hz, which might be related to short wave characteristics of the defect.

From the simulation of the artificial defect with uniform lateral profile can be concluded that the results of the FE simulations are coherent in most of the characteristics (location of the most important frequencies) with respect to the measurements in both the time and the frequency domains.

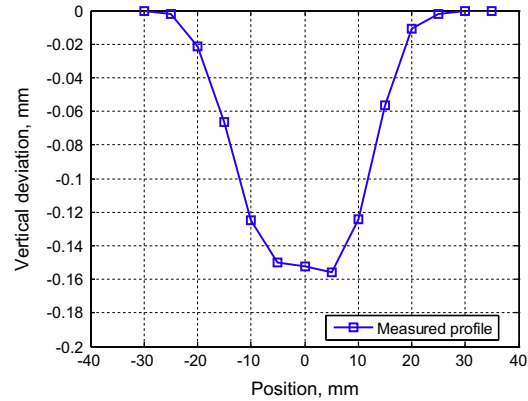
#### 4. Class C squat

##### 4.1. Geometry of a squat

To investigate the ABA response at a defect with non-uniform lateral geometry, a class C squat (Fig. 7a) was simulated with the FE model described above. The measured vertical–longitudinal profile of the simulated squat is shown in Fig. 7b. The measurements of lateral profile were not available for this squat; therefore it was modelled as uniform in the lateral direction, by moving the vertical–longitudinal profile across the rail top. Although the lateral profile of squats is non-uniform, in [13] it was shown that the wavelength of ABA at a defect with uniform lateral profile is the same as the one of parabolic lateral profile. However, the magnitude of ABA is influenced by the lateral profile, and by variations



(a)

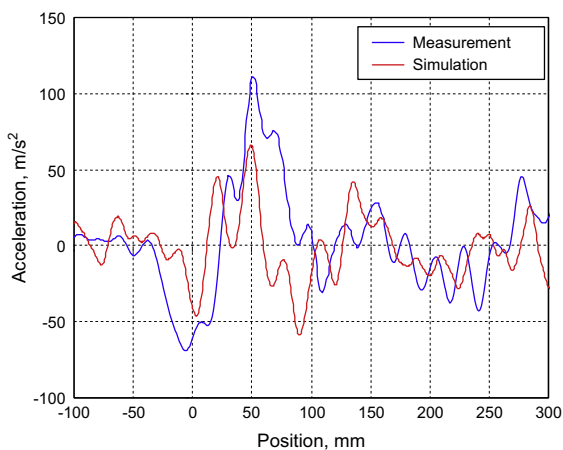


(b)

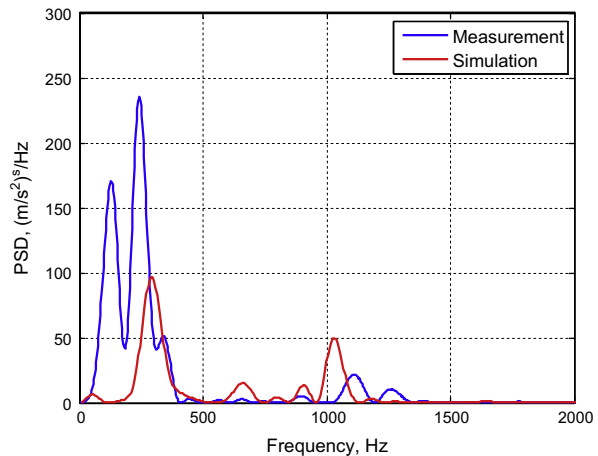
Fig. 7. A class C squat. (a) A photo of a class C squat. (b) Measurements of vertical–longitudinal profile of the class C squat.

in the vertical–longitudinal profile; therefore the modelling of the squat as uniform in lateral direction may cause some discrepancies between the measured and simulated ABA magnitude.

The characteristics of mature squats can be seen in Fig. 7a: a two-lung appearance with V-shaped surface crack, rusty dark areas and widened running band [1,5,6]. The corresponding typical W-shape in the vertical–longitudinal profile can, however, only be observed weakly at the bottom of the profile in Fig. 7b. This is because in severe squats the middle part of the W is partly wiped out by the impact–rolling contact. Since the squat was offset to the gage side the typical W-shape was then almost missed completely in the vertical–longitudinal profile measurements, which were performed along the centre of the rail. Taking the W-shape into



(a)



(b)

Fig. 8. ABA measurements and simulation at squat class C with original profile. (a) ABA. (b) PSD of ABA.

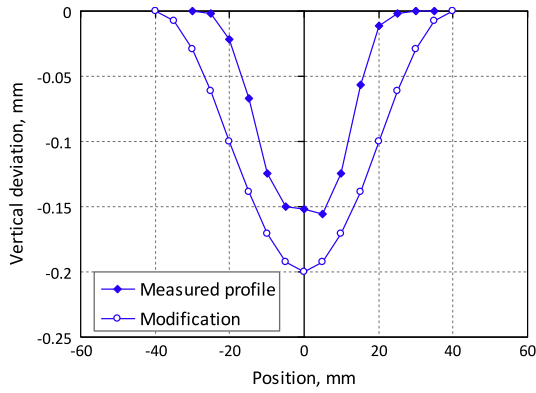


**Fig. 9.** Vertical-longitudinal profile of the class C squat: measurement and its modification.

account, the average wavelength of the squat and the following wave is 28 mm.

4.2. Comparison of the measured and the calculated ABA

The two measured ABA signals at the class C squat were very well repeated; therefore, only one signal with the simulated ABA will be compared. The sampling frequency of ABA measurements is 25 kHz, and the low-pass filter applied to the raw signal had a cut-off frequency of 2 kHz. The comparison between the measured ABA and the simulated ABA is shown in Fig. 8a. The amplitude of the calculated ABA is lower than the measured one between -30 mm and 100 mm; while after 100 mm the calculated amplitude agrees with the measurements. The maximum magnitude of the calculated ABA is about 60% of the one of the measured ABA.

The PSD of the measured and calculated ABA are shown Fig. 8b. The ABA response to the squat is characterized by two main frequencies: about 130–320 Hz, which corresponds to the wavelength of 90–310 mm for the travelling speed of 30–40 m/s, and about 1030–1130 Hz, which corresponds to the wavelength of 26–39 mm. These two frequencies can be used for detection of squats.

There are some discrepancies in the PSD: the power spectrum of the measured ABA is much higher than the one of measured ABA around 130–320 Hz; the measured ABA contains also the frequency at about 130 Hz.

The difference between measurements and simulations may have several reasons. For example, the profile of the squat was not measured accurately. The cracks in the subsurface cause that the measured depth of the squat is smaller than that a passing wheel will actually experience; the modelled lateral geometry was uniform while in reality is not; the track parameters used in simulations were nominal, while in reality the track may had degraded; other factors which were not modelled, including, for example, cracks in the subsurface of the squat.

If the differences between the measurements and simulations were caused by deviation of the measured rail profile from the real one, better agreement can be achieved by adjusting the vertical-longitudinal profile in the model. The adjustments of the profile of the squat are discussed in the next section.

4.3. Adjustment of the vertical-longitudinal profile of the squat

It is possible that the difference in magnitudes of the measured and calculated ABA in Fig. 8 was caused by large deviation of the measured vertical-longitudinal profile of the squat from the real one. Apart from the effect of the cracks, it may also be because the measurements were made on the centre line of the rail, while the squat lied with an offset on the side of the rail. Therefore, the deepest part of the squat was not on the centre line. The length of the dark spot at the squat in Fig. 7a is 57 mm, which is in agreement with the length of the measured profile in Fig. 7b. However, the wear of the rail surface is longer than the measured profile; see the wave of 27 mm in Fig. 7a. Thus, the real profile of the squat might be deeper and longer than the measured profile.

To reduce the difference between the real profile of the squat and the modelled one, some geometry modifications were introduced. With the modifications the profile was made deeper and longer than the measured one (see Modification in Fig. 9).

The difference between the maximum magnitude of the calculated ABA and the measured ABA is still about 60% in Fig. 10a. This is because the ABA is also influenced by the factors discussed above, such as lateral profile of the squat, track parameters, cracks, which were not taken into account.

The ABA in the frequency domain is shown in Fig. 10b. The power spectrum of the calculated ABA around 300 Hz is in a good agreement with the measurements now. It is observed that with the increase of the severity of a squat, the frequency content around 300 Hz become more pronounced. The power of this frequency may therefore be used for assessment of severity of squats.

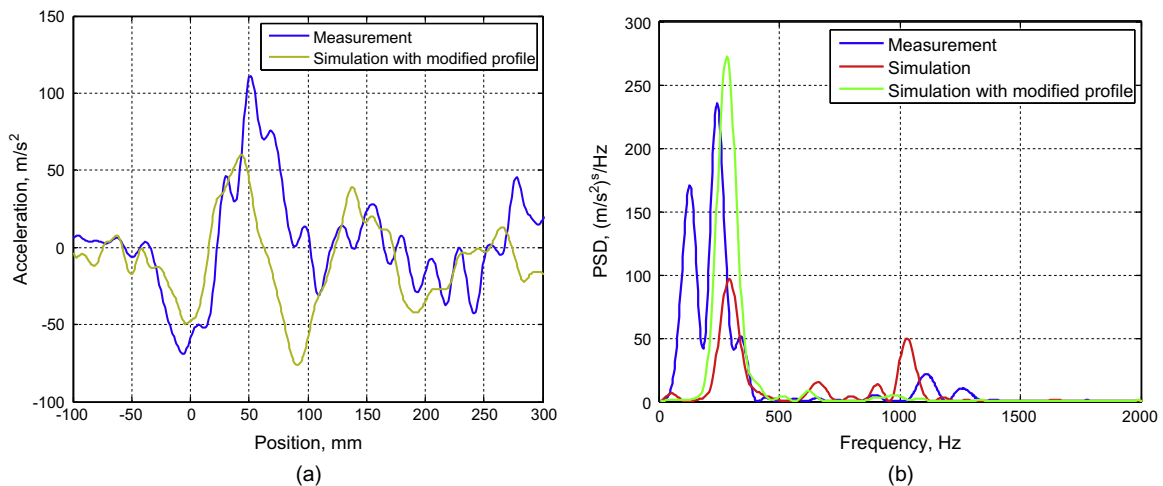


**Fig. 10.** ABA measurements and simulation at squat class C with modified profile. (a) ABA. (b) PSD of ABA.

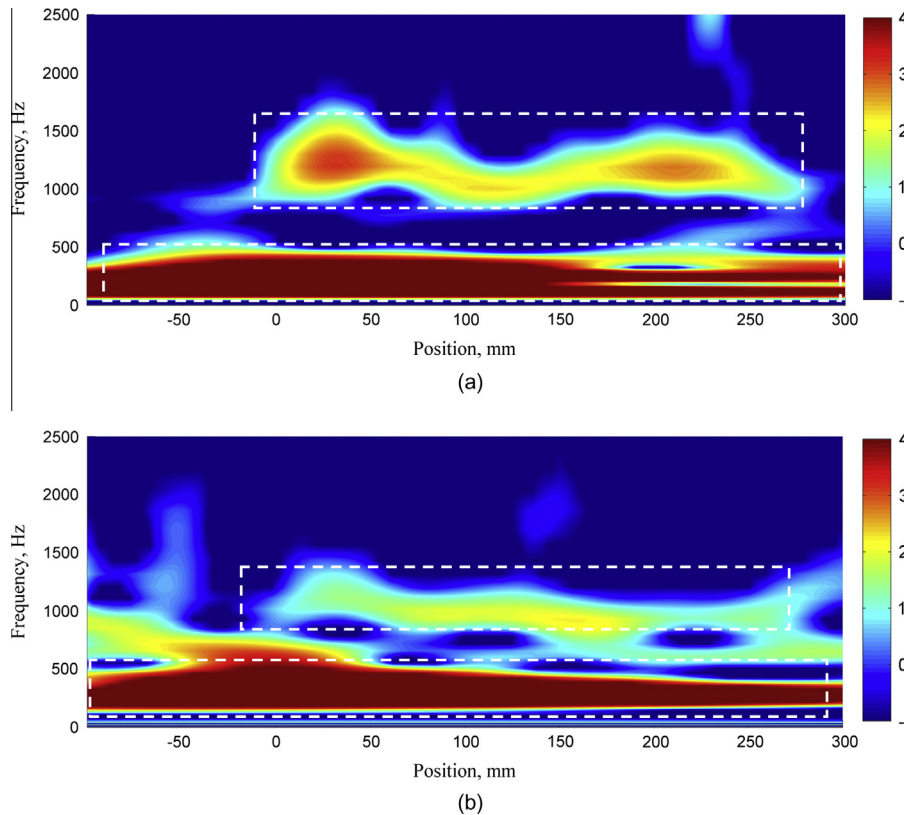


Fig. 11. Wavelet power spectrum of measured (a) and calculated (b) ABA at squat class C.

There are some discrepancies in the PSD: the power spectrum of the calculated ABA is lower than the one of measured ABA around 1030–1130 Hz. It means that with the increase of the severity of a squat the frequency content around 1030–1130 Hz become less pronounced.

The measured ABA contains also the frequency at about 130 Hz which was not observed in the simulations. This discrepancy may be attributed to the difference in track parameters used for the simulation and those in the reality: used are nominal values while in track the parameters can be very probably changed due to damages caused by the impact at the squat.

WPS of the measured and calculated ABA are shown in Fig. 11. At the moment of the impact at the defect (around zero position) frequency up to 1500 can be observed. The two main frequencies discussed above can clearly be seen. Compared with Fig. 5, the length of the lower frequency part is much extended in Fig. 11. This is because the defect in Fig. 11 is much larger than the artificial defect so that more lower frequency vibration is excited, and because under the large impact of the wheel passages the local track system was much disturbed and degraded. Such degradation extends in both directions of the track at the squat. Therefore the major energy is below 550 Hz (see the red area of the plots), and the high frequency part is less pronounced. Nevertheless, there is high frequency part around 1000 Hz which should be associated with a natural frequency of the track. This frequency is responsible for formation of the corrugation-like wave pattern that usually follows squats.

## 5. Conclusions

A FE model was developed and applied for simulations of ABA at two short track defects, a light artificial defect with uniform lateral geometry and a severe squat. The calculated ABA was compared

with measured ones in the frequency range up to 2 kHz because the expected frequencies related to rail top defects are in this frequency range.

The FE model was validated by ABA measurements: it can reproduce the major characteristics of the wheel–track interaction at short track defects and can therefore be used for further investigation of the relation between ABA and short track defects.

In summary, the employed model is suitable for obtaining the relationship between squats and ABA in both temporal and frequency domains. In further work, by simulation of a number of light and moderate squats, the peaks of ABA and its local frequency characteristics may be quantitatively related to the length of the defect. ABA measurements may be employed not only for detection, but also for assessment of severity of squats. Detection of squats, and design of key performance indicators for condition monitoring of rail with squats can be designed with the assistance of the model under controlled simulation based scenarios.

## References

- [1] Li Z, Dollevoet R, Molodova M, Zhao X. Squat growth – some observations and the validation of numerical predictions. *Wear* 2011;271(1):148–57.
- [2] UIC Code, Rail Defects, 4th ed. Paris: International Union of Railways; 2002.
- [3] Smulders J. Management and research tackle rolling contact fatigue. *Railway Gazette Int* 2003:439–42.
- [4] Clayton P, Allery M. Metallurgical aspects of surface damage problems in rails. *Can Metall Quart* 1982;21(1):31–46.
- [5] Rail Damages, The Blue Book of RailTrack. UK; 2001.
- [6] Li Z, Zhao X, Esveld C, Dollevoet R, Molodova M. An investigation into the causes of squats—correlation analysis and numerical modeling. *Wear* 2008;265(9):1349–55.
- [7] Kondo K, Yoroizaka K, Sato Y. Cause, increase, diagnosis, countermeasures and elimination of Shinkansen shelling. *Wear* 1996;191(1):199–203.
- [8] Peng D, Jones R. Modelling of the lock-in thermography process through finite element method for estimating the rail squat defects. *Eng Fail Anal* 2003;28:275–88.

- [9] Boccione M, Caprioli A, Cigada A, Collina A. A measurement system for quick rail inspection and effective track maintenance strategy. *Mech Syst Signal Process* 2007;21(3):1242–54.
- [10] Massel A. Power spectrum analysis—modern tool in the study of rail surface corrugations. *NDT and E Int* 1999;32(8):429–36.
- [11] Caprioli A, Cigada A, Raveglia D. Rail inspection in track maintenance: a benchmark between the wavelet approach and the more conventional Fourier analysis. *Mech Syst Signal Process* 2007;21(2):631–52.
- [12] Remennikov AM, Kaewunruen S. A review of loading conditions for railway track structures due to train and track vertical interaction. *Struct Contr Health Mon* 2008;15(2):207–34.
- [13] Molodova M, Li Z, Dollevoet R. Axle box acceleration: measurement and simulation for detection of short track defects. *Wear* 2011;271(1):349–56.
- [14] Li Z, Molodova M, Zhao X, Dollevoet R. Squat treatment by way of minimum action based on early detection to reduce life cycle costs. In: *Proceedings of the 2010 joint rail conference JRC2010, Urbana-Champaign, Illinois, USA; April 27–29, 2010*.
- [15] Gry L, Gontier C. Dynamic modelling of railway track: a periodic model based on a generalized beam formulation. *J. Sound Vib.* 1997;199–4:531–58.
- [16] Hiensch M, Nielsen JCO, Verheijen E. Rail corrugation in the Netherlands—measurements and simulations. *Wear* 2002;253(1):140–9.
- [17] Bowe C, Mullarkey T. Wheel–rail contact elements incorporating irregularities. *Adv Eng Softw* 2005;36–11:827–37.
- [18] Wen Z, Xiao G, Xiao X, Jin X, Zhu M. Dynamic vehicle–track interaction and plastic deformation of rail at rail welds. *Eng Fail Anal* 2009;16(4):1221–37.
- [19] Meli E, Magheri S, Malvezzi M. Development and implementation of a differential elastic wheel–rail contact model for multibody applications. *Vehicle Syst Dynam* 2011;49(6):969–1001.
- [20] Pletz M, Daves W, Ossberger H. A wheel passing a crossing nose: dynamic analysis under high axle loads using finite element modelling. *Proc Inst Mech Eng Part F: J of Rail Rapid Transit* 2012;226(6):603–11.
- [21] De Man AP. DYNATRACK A survey of dynamic railway track properties and their quality [Ph.D. thesis]. Road and railway engineering section, delft university of technology, The Netherlands, ISBN 90-407-2355-9; 2002. p. 236.
- [22] Hiensch M, Nielsen JCO, Verheijen E. Rail corrugation in The Netherlands—measurements and simulations. *Wear* 2002;253(1):140–9.
- [23] Knothe K, Wu Y. Receptance behaviour of railway track and subgrade. *Arch Appl Mech* 1998;68(7–8):457–70.
- [24] Courant R, Friedrichs K, Lewy H. On the partial difference equations of mathematical physics. *Math Ann* 1928;100:32–74.
- [25] Benson DJ, Hallquist JO. A single surface contact algorithm for the post-buckling analysis of shell structures. *Comput Methods Appl Mech Eng* 1990;78(2):141–63.
- [26] Hlawatsch F, Boudreaux-Bartels G. Linear and quadratic time-frequency signal representations. *IEEE Signal Process Mag* 1992;9(2):21–67.
- [27] Vetterli M, Kovačević J. *Wavelets and Subband Coding*. Prentice Hall, Signal Processing Series. Englewood Cliffs, NJ; 1995.
- [28] Belšak A, Flašker J. Methods for detecting fatigue cracks in gears. *J Phys: Conf Ser* 2009;181:012090.
- [29] Ovanosova AV, Suárez LE. Applications of wavelet transforms to damage detection in frame structures. *Eng Struct* 2004;26–1:39–49.
- [30] Liew KM, Wang Q. Application of wavelet theory for crack identification in structures. *J Eng Mech* 1998;124–2:152–7.
- [31] Wang Q, Deng X. Damage detection with spatial wavelets. *Int J Solids Struct* 1999;36(23):3443–68.